

A Sequential Coupling of Optimal Topology and Multilevel Shape Design Applied to 2-Dimensional Nonlinear Magnetostatics *

Dalibor Lukáš[†], Pavel Chalmovianský[‡]

May 20, 2005

Abstract

In this paper, a sequential coupling of 2-dimensional optimal topology and shape design is proposed so that a coarsely discretized and optimized topology is the initial guess for the following shape optimization. In between, we approximate the optimized topology by piecewise Bézier shapes via least square fitting. For the topology optimization, we use the steepest descent method. The state problem is a nonlinear Poisson equation discretized by the finite element method and eliminated within Newton iterations, while the particular linear systems are solved using a multigrid preconditioned conjugate gradients method. The shape optimization is also solved in a multilevel fashion, where at each level the sequential quadratic programming is employed. We further propose an adjoint sensitivity analysis method for the nested nonlinear state system. At the end, the machinery is applied to optimal design of a direct electric current electromagnet. The results correspond to physical experiments.

Keywords: topology optimization, shape optimization, sensitivity analysis, finite element method, multigrid, magnetostatics

1 Introduction

In the process of development of industrial components, one looks for the parameters to be optimal subject to a proper criterion. The geometry is usually

*This research has been supported by the Austrian Science Fund FWF within the SFB “Numerical and Symbolic Scientific Computing” under the grant SFB F013, subprojects F1309 and F1315, by the Czech Ministry of Education under the grant AVČR 1ET400300415, by the Czech Grant Agency under the grant GAČR 201/05/P008 and by the Slovak Grant Agency under the project VEGA 1/0262/03.

[†]Department of Applied Mathematics, VŠB–Technical University of Ostrava, Czech Republic, email: dalibor.lukas@vsb.cz

[‡]Special Research Programme SFB F013 “Numerical and Symbolic Scientific Computing”, University of Linz, Austria, email: pavel.chalmoviansky@sfb013.uni-linz.ac.at

crucial when the design of electromagnetic components is concerned. We can employ topology optimization, cf. [Ben95], to find an optimal distribution of the material without any preliminary knowledge. However, this is very computationally expensive due to the large number of design variables. On the other hand, shape optimization, cf. [HN97, SZ92], is used to tune shapes of a known initial design the topology of which cannot be changed. Due to the relatively small number of design variables, shape optimization proceeds significantly faster. The idea here is to couple both sequentially.

In [Cea00], a connection between topological and shape gradient is shown and applied in structural mechanics. They proceed shape and topology optimization simultaneously so that at each optimization step both the shape and topology gradient are calculated. Then shapes are displaced and the elements with great values of the topology gradient are removed, while introducing the natural boundary condition along the new parts, e.g. a hole. Here we are rather motivated by the approach in [OBR91, TCh01], where they proceed shape optimization after topology optimization and the algorithm is applied to structural mechanics. However, they used re-meshing in a robust CAD software environment, which was computationally very expensive. Our aim here is to make the algorithm fast. Therefore, we additionally employ semianalytical sensitivity analysis and a multilevel method. An important issue in this approach is a proper geometrical modeling, cf. [Far96]. We use Bézier parametric representation of the shapes to be finally optimized.

We consider solution of optimization problems by steepest descent or Newton-type methods. Additionally to the cost functional, the gradient has to be evaluated. One can use a numerical differentiation scheme, which is very robust, but the computational effort is proportional to the number of design variables times the effort for the cost functional. There is also an automatic differentiation approach, cf. [Gri00], where the code of the evaluation of the cost functional is automatically transferred to the code for the gradient calculation. This is very robust, but extremely both memory and time consuming when not exploiting the structure of the large-scale problem under consideration. As far as a partial differential (PDE) state problem is involved, it is recommended to use semi-analytical methods, cf. [HCK86], where the gradient of the cost functional is about that expensive to evaluate as the cost functional itself. However, up to the authors' knowledge, nonlinear smooth material behaviour is hardly considered, which seems to be due to a bit more technical programming issues. In this paper, we derive general algorithms and formulas in a very detail for both topology and shape sensitivity analysis when considering nested evaluation of a smooth nonlinear PDE state problem. Note that it is proper to combine the semianalytical methods with numerical or automatic differentiation applied to small-scale subproblems only.

As mentioned above, we use a multigrid approach. It has already become a standard solution method for discretized PDE systems. The method properly solves the problem discretized on a hierarchy of grids while eliminating different scales of eigenfrequencies of the PDE operator separately. This makes the convergence rate to be optimal with respect to the number of degrees of free-

dom. The analysis as well as applications can be found in [Hac85, Bra93, JL85]. Recently, there has been a growing interest in a multilevel solution to nonlinear, especially, optimization problems. One can use a simultaneous approach with a successive linearizations of Karush-Kuhn-Tucker system involving the state problem as a constraint, thus, doing both design and state updates simultaneously. In [SMS00], a multilevel optimization for this approach is presented. Here, we are concerned with a nested approach, where the state solution is eliminated and then plugged into the outer optimal design process. We develop a multilevel approach for this.

The paper is organized as follows. In Section 2, we state the topology optimization problem governed with a 2-dimensional nonlinear Poisson equation, we discretize it by finite elements, use Newton method to eliminate the state problem and we derive a so-called adjoint Newton method for calculating the topology gradient. In Section 3, the sequential coupling between topology and shape optimization is described. Using the least square fitting, we approximate the coarsely optimized topology with a domain the boundary of which is given as a set of Bézier curves. In Section 4, the arising shape optimization problem is presented. Similarly to the topology optimization case, we derive the adjoint Newton algorithm. We further propose a multilevel algorithm for the shape optimization, making use of an efficient preconditioning to the state problem. In Section 5, an application to a direct electric current electromagnet is given. In Section 6, we present numerical results in terms of the computational effort. We conclude in Section 7.

2 Topology optimization for magnetostatics

Let us consider a sufficiently regular fixed computational domain $\Omega \subset \mathbb{R}^2$, where domain stands for a nonempty, open and simply connected set. We will deal with a 2-dimensional (2d) nonlinear magnetostatics, which can be described by the following Poisson boundary value problem:

$$\begin{cases} -\operatorname{div}(\nu(\mathbf{x}, \|\mathbf{grad}(u(\mathbf{x}))\|^2)\mathbf{grad}(u(\mathbf{x}))) & = J(\mathbf{x}) & \text{in } \Omega \\ u(\mathbf{x}) & = 0 & \text{on } \partial\Omega \end{cases}, \quad (1)$$

where u denotes a scalar magnetic potential so that $(\partial u/\partial x_2, -\partial u/\partial x_1)$ is a magnetic field density, ν is a magnetic reluctivity, which is bounded from 0 by the air reluctivity $\nu_0 > 0$ and which is considered to be nonlinearly dependent on $\|\mathbf{grad}(u)\|^2$ in ferromagnetic parts. Finally, J denotes an electric current density. We will formulate the problem (1) weakly in the Sobolev space $H_0^1(\Omega)$.

In this paper, we are interested in an inverse problem to (1), namely, we are looking for an optimal design of the ferromagnetic parts, i.e. for an optimal distribution of the reluctivity function ν . Let $\Omega_d \subset \Omega$ be the subdomain where the designed structure can arise. The set of admissible material distributions is denoted by $\mathcal{Q} := \{\rho \in L^2(\Omega_d) \mid 0 \leq \rho \leq 1\}$. We penalize the intermediate

values by

$$\tilde{\rho}(\rho) \equiv \tilde{\rho}_{p_\rho}(\rho) := \frac{1}{2} \left(1 + \frac{1}{\arctan(p_\rho)} \arctan(p_\rho(2\rho - 1)) \right),$$

where $p_\rho := 100$ is typically good enough. From now on, we will consider the nonlinear magnetic reluctivity in the following form:

$$\nu(\eta, \tilde{\rho}) := \begin{cases} \nu_0 + (\nu(\eta) - \nu_0)\tilde{\rho}, & \text{in } \Omega_d \\ \nu_0, & \text{otherwise,} \end{cases} \quad (2)$$

where $\nu(\eta) := \nu_1 + (\nu_0 - \nu_1)\frac{\eta^4}{\eta^4 + \nu_0^{-1}}$ and $\nu_0 := 1/(4\pi 10^{-7})$ [mH⁻¹], $\nu_1 > 0$ are the constant reluctivities of the air and ferromagnetics, respectively. Finally, let $\mathcal{I} : H^1(\Omega) \rightarrow \mathbb{R}$ be a cost functional. Given a maximal volume V_{\max} of the designed structure, the 2d topology optimization problem governed by the nonlinear magnetostatics then reads as follows:

$$\begin{cases} \min_{\rho \in \mathcal{Q}} \left(\mathcal{I}(u) + p_V \max \left\{ \int_{\Omega_d} \tilde{\rho}(\rho) - V_{\max}, 0 \right\}^2 \right) \\ \text{w.r.t.} \\ \int_{\Omega} \mathbf{grad}(v) \nu(\|\mathbf{grad}(u)\|^2, \tilde{\rho}(\rho)) \mathbf{grad}(u) \, d\mathbf{x} = \int_{\Omega} Jv \, d\mathbf{x} \text{ in } H_0^1(\Omega), \end{cases} \quad (3)$$

where $p_V \gg 0$ is a penalty of the maximal volume constraint and $J \in L^2(\Omega)$ is a current density.

2.1 Numerical solution

The problem (3) is discretized by the finite element method using the linear Lagrange elements on triangles. The design material distribution is elementwise constant. This leads to the following nonlinear system of equations:

$$\mathbf{A}(\mathbf{u}, \tilde{\rho}) \mathbf{u} = \mathbf{f},$$

where $\mathbf{u} \in \mathbb{R}^n$ and $\tilde{\rho} \in \mathbb{R}^m$ are the vector counterparts of the discretized solution u and the penalized design $\tilde{\rho}$, respectively, and where n, m denote the numbers of the nodes and of the elements, respectively. We apply a nested approach, where the outer optimization is solved within steepest-descent iterations and the nested magnetostatic problem is eliminated by the Newton method, as described in Algorithm 1 below. We denote by $I : \mathbb{R}^n \times \mathbb{R}^m \rightarrow \mathbb{R}$ the discretized cost functional \mathcal{I} including the penalty term, see (3), and by $\mathbf{A}'_{\mathbf{u}}(\mathbf{u}, \tilde{\rho})$ the linearization of the matrix $\mathbf{A}(\mathbf{u}, \tilde{\rho})$. Since we consider only one coarse discretization, the particular linear systems in Algorithm 1 are solved directly. In the optimization, we choose the initial value of ρ to be 0.5.

At the beginning of Algorithm 1, the linear state problem is solved, which results in a proper approximation \mathbf{u}^0 of the solution. Then, we compute the defect. The algorithm further proceeds in Newton iterations, where the main

step is a solution to a linear system $\mathbf{A}'_{\mathbf{u}}$, which is the operator \mathbf{A} linearized at the current solution approximation \mathbf{u}^{i-1} , with the defect being the right-hand side. This gives us an update direction \mathbf{w}^i of the solution \mathbf{u}^{i-1} and we perform a simple line-search to find an optimal step τ^i in the direction \mathbf{w}^i . Then, both the solution approximation and the defect are updated and the algorithm proceeds until the defect is sufficiently small with respect to the original right-hand side.

Algorithm 1 State problem solver for topology optimization

Given $\boldsymbol{\rho}, \tilde{\boldsymbol{\rho}} := \tilde{\boldsymbol{\rho}}(\boldsymbol{\rho})$
 $i := 0$
Solve $\mathbf{A}(\mathbf{0}, \tilde{\boldsymbol{\rho}}) \mathbf{u}^0 = \mathbf{f}$
Assemble $\mathbf{f}^0 := \mathbf{f} - \mathbf{A}(\mathbf{u}^0, \tilde{\boldsymbol{\rho}}) \mathbf{u}^0$
while $\|\mathbf{f}^i\|/\|\mathbf{f}\| > \text{precision}$ **do**
 $i := i + 1$
Solve $\mathbf{A}'_{\mathbf{u}}(\mathbf{u}^{i-1}, \tilde{\boldsymbol{\rho}}) \mathbf{w}^i = \mathbf{f}^{i-1}$
Find τ^i : $\|\mathbf{f} - \mathbf{A}(\mathbf{u}^{i-1} + \tau^i \mathbf{w}^i, \tilde{\boldsymbol{\rho}}) (\mathbf{u}^{i-1} + \tau^i \mathbf{w}^i)\| < \mathbf{f}^{i-1}$
 $\mathbf{u}^i := \mathbf{u}^{i-1} + \tau^i \mathbf{w}^i$
 $\mathbf{f}^i := \mathbf{f} - \mathbf{A}(\mathbf{u}^i, \tilde{\boldsymbol{\rho}}) \mathbf{u}^i$
Store \mathbf{w}^i and τ^i
end while
Store \mathbf{u}^i
Store $k := i$
Calculate objective $I(\mathbf{u}^k, \tilde{\boldsymbol{\rho}})$

Now, we will describe assembling the linear systems that appear in Algorithm 1. The matrix $\mathbf{A}(\mathbf{u}, \tilde{\boldsymbol{\rho}})$ is summed over triangular elements K^e with the following local contributions:

$$\mathbf{A}^e(\mathbf{u}^e, \tilde{\boldsymbol{\rho}}^e) := \int_{K^e} \mathbf{B}^e(\mathbf{x})^T \nu(\|\mathbf{B}^e(\mathbf{x}) \mathbf{u}^e\|^2, \tilde{\boldsymbol{\rho}}^e) \mathbf{B}^e(\mathbf{x}) dx,$$

where

$$\mathbf{B}^e(\mathbf{x}) := [\mathbf{grad}(\xi_1^e(\mathbf{x})), \mathbf{grad}(\xi_2^e(\mathbf{x})), \mathbf{grad}(\xi_3^e(\mathbf{x}))], \quad \mathbf{B}^e(\mathbf{x}) \mathbf{u}^e = \mathbf{grad}(u(\mathbf{x}))|_{K^e},$$

where ξ_1^e , ξ_2^e and ξ_3^e are linear shape functions related to the corners \mathbf{x}_1^e , \mathbf{x}_2^e and \mathbf{x}_3^e of the triangle K^e . Now, we replace the integration over K^e by the integration over a reference triangle K^r with the corners $(0,0)^T$, $(1,0)^T$ and $(0,1)^T$ and we arrive at the formula

$$\mathbf{A}^e(\mathbf{u}^e, \tilde{\boldsymbol{\rho}}^e) = (\mathbf{B}^e)^T \nu(\|\mathbf{B}^e \mathbf{u}^e\|^2, \tilde{\boldsymbol{\rho}}^e) \mathbf{B}^e \frac{|\det(\mathbf{R}^e)|}{2}, \quad (4)$$

where

$$\mathbf{B}^e = (\mathbf{R}^e)^{-T} \mathbf{B}^r, \quad \mathbf{R}^e := [\mathbf{x}_3^e - \mathbf{x}_1^e, \mathbf{x}_2^e - \mathbf{x}_1^e], \quad \mathbf{B}^r := \begin{bmatrix} -1 & 1 & 0 \\ -1 & 0 & 1 \end{bmatrix}.$$

The matrix \mathbf{B}^r contains the gradients of the linear shape functions over the reference triangle K^r . Adopting this notation, the linearization $\mathbf{A}'_{\mathbf{u}}(\mathbf{u}, \tilde{\boldsymbol{\rho}})$ is also assembled elementwise with the following local contributions:

$$\begin{aligned} \mathbf{A}'_{\mathbf{u}^e}(\mathbf{u}^e, \tilde{\boldsymbol{\rho}}^e) &= (\mathbf{B}^e)^T \left\{ \left[\nu(\|\mathbf{B}^e \mathbf{u}^e\|^2, \tilde{\boldsymbol{\rho}}^e) \mathbf{I} \right. \right. \\ &\quad \left. \left. + 2\nu'_{\eta^e}(\|\mathbf{B}^e \mathbf{u}^e\|^2, \tilde{\boldsymbol{\rho}}^e) (\mathbf{B}^e \mathbf{u}^e) (\mathbf{B}^e \mathbf{u}^e)^T \right] \mathbf{B}^e \right\} \frac{|\det(\mathbf{R}^e)|}{2}, \end{aligned} \quad (5)$$

where \mathbf{I} denotes the unit matrix and $\nu'_{\eta^e}(\eta^e, \tilde{\boldsymbol{\rho}}^e)$ is the derivative of ν w.r.t. η^e .

2.2 Topology sensitivity analysis

Here, a large number of design variables would cause a costly Hessian approximation. Therefore, in the very outer optimization, rather than a quasi-Newton iterations we use the steepest-descent method. We have to provide the derivative of the cost functional I subject to the elementwise constant design material function $\boldsymbol{\rho}$. To this end, we analytically differentiate Algorithm 1 in the backward way, which results in Algorithm 2. Additionally, we introduce the following matrices:

$$\begin{aligned} \mathbf{G}_{\tilde{\boldsymbol{\rho}}}(\mathbf{u}, \mathbf{w}, \tilde{\boldsymbol{\rho}}) &:= - \left(\frac{\partial \mathbf{A}'_{\mathbf{u}}(\mathbf{u}, \tilde{\boldsymbol{\rho}})}{\partial \rho_1} \mathbf{w}, \dots, \frac{\partial \mathbf{A}'_{\mathbf{u}}(\mathbf{u}, \tilde{\boldsymbol{\rho}})}{\partial \rho_m} \mathbf{w} \right) \\ &\quad - \left(\frac{\partial \mathbf{A}(\mathbf{u}, \tilde{\boldsymbol{\rho}})}{\partial \rho_1} \mathbf{u}, \dots, \frac{\partial \mathbf{A}(\mathbf{u}, \tilde{\boldsymbol{\rho}})}{\partial \rho_m} \mathbf{u} \right), \end{aligned}$$

$$\begin{aligned} \mathbf{G}_{\mathbf{u}}(\mathbf{u}, \mathbf{w}, \tilde{\boldsymbol{\rho}}) &:= - \left(\frac{\partial \mathbf{A}'_{\mathbf{u}}(\mathbf{u}, \tilde{\boldsymbol{\rho}})}{\partial u_1} \mathbf{w}, \dots, \frac{\partial \mathbf{A}'_{\mathbf{u}}(\mathbf{u}, \tilde{\boldsymbol{\rho}})}{\partial u_n} \mathbf{w} \right) \\ &\quad - \left(\frac{\partial \mathbf{A}(\mathbf{u}, \tilde{\boldsymbol{\rho}})}{\partial u_1} \mathbf{u}, \dots, \frac{\partial \mathbf{A}(\mathbf{u}, \tilde{\boldsymbol{\rho}})}{\partial u_n} \mathbf{u} \right) - \mathbf{A}(\mathbf{u}, \tilde{\boldsymbol{\rho}}), \end{aligned}$$

$$\mathbf{H}_{\tilde{\boldsymbol{\rho}}}(\mathbf{u}, \tilde{\boldsymbol{\rho}}) := - \left(\frac{\partial \mathbf{A}(\mathbf{0}, \tilde{\boldsymbol{\rho}})}{\partial \rho_1} \mathbf{u}, \dots, \frac{\partial \mathbf{A}(\mathbf{0}, \tilde{\boldsymbol{\rho}})}{\partial \rho_m} \mathbf{u} \right).$$

From (2), (4) and (5) it is easy to see that the only elementwise contributions to the matrices $\mathbf{G}_{\mathbf{u}}(\mathbf{u}, \mathbf{w}, \tilde{\boldsymbol{\rho}})$ and $\mathbf{H}_{\tilde{\boldsymbol{\rho}}}(\mathbf{u}, \tilde{\boldsymbol{\rho}})$ reads as follows:

$$\frac{\partial \mathbf{A}'_{\mathbf{u}^e}(\mathbf{u}^e, \tilde{\boldsymbol{\rho}}^e)}{\partial \rho^e} \mathbf{w}^e = \mathbf{A}'_{\mathbf{u}^e}(\mathbf{u}^e, 1) \mathbf{w}^e \quad \text{and} \quad \frac{\partial \mathbf{A}(\mathbf{u}^e, \tilde{\boldsymbol{\rho}}^e)}{\partial \rho^e} \mathbf{u}^e = \mathbf{A}(\mathbf{u}^e, 1) \mathbf{u}^e.$$

The elementwise contributions to $\mathbf{G}_{\mathbf{u}}(\mathbf{u}, \mathbf{w}, \tilde{\boldsymbol{\rho}})$ are a bit more involved:

$$\begin{aligned} \mathbf{G}_{\mathbf{u}^e}(\mathbf{u}^e, \mathbf{w}^e, \tilde{\boldsymbol{\rho}}^e) := & -(\mathbf{B}^e)^T \left\{ \frac{\nu^{e'}(\|\mathbf{B}^e \mathbf{u}^e\|^2)}{\|\mathbf{B}^e \mathbf{u}^e\|} \left[\|\mathbf{B}^e \mathbf{u}^e\| \|\mathbf{B}^e \mathbf{w}^e\| \mathbf{I} + (\mathbf{B}^e \mathbf{u}^e)(\mathbf{B}^e \mathbf{w}^e)^T \right. \right. \\ & \left. \left. + (\mathbf{B}^e \mathbf{w}^e)(\mathbf{B}^e \mathbf{u}^e)^T \right] \right. \\ & + \left(\frac{\nu^{e''}(\|\mathbf{B}^e \mathbf{u}^e\|^2)}{\|\mathbf{B}^e \mathbf{u}^e\|^2} - \frac{\nu^{e'}(\|\mathbf{B}^e \mathbf{u}^e\|^2)}{\|\mathbf{B}^e \mathbf{u}^e\|^3} \right) \\ & \times \|\mathbf{B}^e \mathbf{u}^e\| \|\mathbf{B}^e \mathbf{w}^e\| (\mathbf{B}^e \mathbf{u}^e)(\mathbf{B}^e \mathbf{u}^e)^T \\ & \left. + \nu^e(\|\mathbf{B}^e \mathbf{u}^e\|^2) \mathbf{I} \right\} \mathbf{B}^e \frac{|\det(\mathbf{R}^e)|}{2}, \end{aligned} \quad (6)$$

where $\nu^e(\eta^e) := \nu(\eta^e, \tilde{\boldsymbol{\rho}}^e)$, $\nu^{e'}(\eta^e) := \nu'_{\eta^e}(\eta^e, \tilde{\boldsymbol{\rho}}^e)$ and $\nu^{e''}(\eta^e) := \nu''_{\eta^e \eta^e}(\eta^e, \tilde{\boldsymbol{\rho}}^e)$.

Algorithm 2 Adjoint Newton method for topology optimization

Given $\boldsymbol{\rho}, \tilde{\boldsymbol{\rho}} := \tilde{\boldsymbol{\rho}}(\boldsymbol{\rho}), k, \mathbf{u}^k, \{\mathbf{w}^i\}_{i=1}^k$ and $\{\tau^i\}_{i=1}^k$ stored by Algorithm 1
 $\boldsymbol{\lambda} := I'_{\mathbf{u}}(\mathbf{u}^k, \tilde{\boldsymbol{\rho}})$
 $\boldsymbol{\omega} := \mathbf{0}$
for $i = k, \dots, 1$ **do**
 $\mathbf{u}^{i-1} := \mathbf{u}^i - \tau^i \mathbf{w}^i$
 Solve $\mathbf{A}'_{\mathbf{u}}(\mathbf{u}^{i-1}, \tilde{\boldsymbol{\rho}})^T \boldsymbol{\eta} = \boldsymbol{\lambda}$
 Assemble $\boldsymbol{\omega} := \boldsymbol{\omega} + \tau^i \mathbf{G}_{\tilde{\boldsymbol{\rho}}}(\mathbf{u}^{i-1}, \mathbf{w}^i, \tilde{\boldsymbol{\rho}})^T \boldsymbol{\eta}$
 Assemble $\boldsymbol{\lambda} := \boldsymbol{\lambda} + \tau^i \mathbf{G}_{\mathbf{u}}(\mathbf{u}^{i-1}, \mathbf{w}^i, \tilde{\boldsymbol{\rho}})^T \boldsymbol{\eta}$
end for
Solve $\mathbf{A}(\mathbf{0}, \tilde{\boldsymbol{\rho}})^T \boldsymbol{\eta} = \boldsymbol{\lambda}$
Assemble $\boldsymbol{\omega} := \boldsymbol{\omega} + \mathbf{H}_{\tilde{\boldsymbol{\rho}}}(\mathbf{u}^0, \tilde{\boldsymbol{\rho}})^T \boldsymbol{\eta} + I'_{\tilde{\boldsymbol{\rho}}}(\mathbf{u}^k, \tilde{\boldsymbol{\rho}})$
Calculate the gradient of the objective $I'_{\boldsymbol{\rho}}(\mathbf{u}^k(\tilde{\boldsymbol{\rho}}(\boldsymbol{\rho})), \tilde{\boldsymbol{\rho}}(\boldsymbol{\rho})) := \tilde{\boldsymbol{\rho}}'_{\boldsymbol{\rho}}(\boldsymbol{\rho}) \boldsymbol{\omega}$

3 Smooth shapes fitting

The coarsely discretized optimal topology design serves as the initial guess for the shape optimization. The first step towards a fully automatic procedure is a shape identification. The second step, we are treating now, is a piecewise smooth approximation of the shapes by Bézier curves. It is given as

$$\alpha(\mathbf{p})(t) := \sum_{i=0}^n B_i^n(t) [\mathbf{p}]_i \quad \text{with} \quad B_i^n(t) := \binom{n}{i} (1-t)^{n-i} t^i.$$

We are interested in the arc for $t \in [0, 1]$.

Let $\boldsymbol{\rho}^{\text{opt}} \in \mathcal{Q}$ be an optimized discretized material distribution. Recall that it is not a strictly 0-1 function. Let $\mathbf{p}_1 \in \mathbb{R}^{n_1}, \dots, \mathbf{p}_s \in \mathbb{R}^{n_s}$ denote vectors of Bézier parameters of the shapes $\alpha_1(\mathbf{p}_1), \dots, \alpha_s(\mathbf{p}_s)$ which form the air and ferromagnetic subdomains $\Omega_0(\alpha_1, \dots, \alpha_s)$ and $\Omega_1(\alpha_1, \dots, \alpha_s)$, respectively, i.e.

$\Omega_1 \subset \Omega_d$, $\overline{\Omega} = \overline{\Omega_0} \cup \overline{\Omega_1}$ and $\Omega_0 \cap \Omega_1 = \emptyset$. Let further $\underline{\mathbf{p}}_i$ and $\overline{\mathbf{p}}_i$ denote the lower and upper bounds, respectively, and let

$$\mathcal{P} := \{(\mathbf{p}_1, \dots, \mathbf{p}_s) \mid \underline{\mathbf{p}}_i \leq \mathbf{p}_i \leq \overline{\mathbf{p}}_i \text{ for } i = 1, \dots, s\} \quad (7)$$

be the set of admissible Bézier parameters. We solve the following least square fitting problem:

$$\min_{(\mathbf{p}_1, \dots, \mathbf{p}_s) \in \mathcal{P}} \int_{\Omega_d} (\rho^{\text{opt}} - \chi(\Omega_1(\alpha_1(\mathbf{p}_1), \dots, \alpha_s(\mathbf{p}_s))))^2 dx, \quad (8)$$

where $\chi(\Omega_1)$ is the characteristic function of Ω_1 .

When solving (8) numerically, one encounters a problem of intersection of the Bézier shapes with the mesh on which ρ^{opt} is elementwise constant. In order to avoid it we use the property that the Bézier control polygon converges linearly to the curve under the following refinement procedure:

$$\begin{aligned} [\mathbf{p}_i^{\text{new}}]_1 &:= [\mathbf{p}_i]_1, \\ [\mathbf{p}_i^{\text{new}}]_j &:= \frac{j-1}{n_i+1} [\mathbf{p}_i]_{j-1} + \frac{n-j}{n_i+1} [\mathbf{p}_i]_j, \quad j = 2, \dots, n_i, \\ [\mathbf{p}_i^{\text{new}}]_{n_i+1} &:= [\mathbf{p}_i]_{n_i}, \end{aligned} \quad (9)$$

where $i = 1, \dots, s$. This procedure adds one control node so that the resulting Bézier shape remains unchanged. In Fig. 1 a convergence of control polygons of 6, 11, 21, 41 and 81 nodes to the Bézier shape is depicted. For a faster convergence of control polygon toward a curve, we can use subdivision techniques. The integration in (8) is then replaced by a sum over the elements and we deal

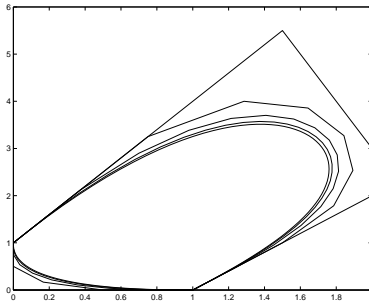


Figure 1: Approximation of Bézier shapes by the refined control polygon

with intersecting of the mesh and a polygon.

Note that the least square functional in (8) is not differentiable whenever a shape touches the grid. Nevertheless, we compute forward finite differences, which is still acceptable for the steepest-descent optimization method that we use. The smoothness can be achieved by smoothing the characteristic function $\chi(\Omega_1)$.

4 Shape optimization for magnetostatics

With the notation of Sect. 2, the shape optimization problem under consideration is as follows:

$$\left\{ \begin{array}{l} \min_{(\mathbf{p}_1, \dots, \mathbf{p}_s) \in \mathcal{P}} \left(\mathcal{I}(u) + p_V \max \left\{ \int_{\Omega_1(\alpha_1(\mathbf{p}_1), \dots, \alpha_s(\mathbf{p}_s))} dx - V_{\max}, 0 \right\} \right)^2 \\ \text{w.r.t.} \\ \int_{\Omega_0(\alpha_1(\mathbf{p}_1), \dots, \alpha_s(\mathbf{p}_s))} \mathbf{grad}(v) \cdot \nu_0 \mathbf{grad}(u) dx \\ + \int_{\Omega_1(\alpha_1(\mathbf{p}_1), \dots, \alpha_s(\mathbf{p}_s))} \mathbf{grad}(v) \cdot \nu(\|\mathbf{grad}(u)\|^2, 1) \mathbf{grad}(u) dx = \int_{\Omega} Jv dx \text{ in } H_0^1(\Omega). \end{array} \right. \quad (10)$$

4.1 Numerical solution

Similarly to the case of topology optimization, we discretize the problem (10) by the finite element method using the linear Lagrange triangular elements. Additionally, the interface $\overline{\Omega_0} \cap \overline{\Omega_1}$ to be optimized is discretized as well for the initial design $\alpha_1^{\text{init}} := \alpha_1(\mathbf{p}_1^{\text{init}})$, \dots , $\alpha_s^{\text{init}} := \alpha_s(\mathbf{p}_s^{\text{init}})$, where $(\mathbf{p}_1^{\text{init}}, \dots, \mathbf{p}_s^{\text{init}})$ is the solution of (8). Let us accumulate all the initial shape coordinates into the vector α^{init} and let the initial grid nodes be denoted by \mathbf{x}^{init} .

Shape perturbations $\Delta \alpha := \alpha - \alpha^{\text{init}}$ are mapped to the grid perturbations $\Delta \mathbf{x} := \mathbf{x} - \mathbf{x}^{\text{init}}$ by solving the following auxiliary linear elasticity problem on the grid \mathbf{x}^{init} with a nonhomogeneous Dirichlet interface condition $\Delta \alpha$ along $\overline{\Omega_0} \cap \overline{\Omega_1}$:

$$(\mathbf{K}^{\text{stiff}}(\mathbf{x}^{\text{init}}) + p_\alpha \mathbf{K}^{\text{robin}}(\mathbf{x}^{\text{init}})) \Delta \mathbf{x} = p_\alpha \mathbf{K}^{\text{robin}}(\mathbf{x}^{\text{init}}) \mathbf{M} \Delta \alpha, \quad (11)$$

where $\mathbf{K}^{\text{stiff}}(\mathbf{x}^{\text{init}})$ is the elasticity stiffness matrix, $\mathbf{K}^{\text{robin}}(\mathbf{x}^{\text{init}})$ is the mass matrix on the interface $\overline{\Omega_0} \cap \overline{\Omega_1}$, \mathbf{M} is a perturbation matrix mapping the shape coordinates to the grid and $p_\alpha \gg 0$ is a penalty forcing the nonhomogeneous Dirichlet interface condition. Note that the drawback of this approach is that on fine meshes some elements may flip whenever the shape changes significantly. In our case, it did not happen due to the multilevel optimization approach, where the fine optimized shapes were already well approximated by the coarse ones.

Now, the nonlinear state equation reads

$$\mathbf{A}(\mathbf{u}, \Delta \mathbf{x}) \mathbf{u} = \mathbf{f},$$

the solution of which is described in Algorithm 3, where, in addition to Algorithm 1, we solve the shape-to-mesh map (11) at the beginning. The element contributions to the system matrix reads as follows:

$$\mathbf{A}^e(\mathbf{u}^e, \Delta \mathbf{x}^e) := (\mathbf{B}^e(\Delta \mathbf{x}^e))^T \nu(\|\mathbf{B}^e(\Delta \mathbf{x}^e) \mathbf{u}^e\|^2, 1) \mathbf{B}^e(\Delta \mathbf{x}^e) \frac{|\det(\mathbf{R}^e(\Delta \mathbf{x}^e))|}{2}, \quad (12)$$

Algorithm 3 State problem solver for shape optimization

Given \mathbf{p} , $\Delta\boldsymbol{\alpha} := \boldsymbol{\alpha}(\mathbf{p}) - \boldsymbol{\alpha}^{\text{init}}$
 Solve $(\mathbf{K}^{\text{stiff}} + p\mathbf{K}^{\text{robin}}) \Delta\mathbf{x} = p\mathbf{K}^{\text{robin}}\mathbf{M}\Delta\boldsymbol{\alpha}$
 $i := 0$
 Solve $\mathbf{A}(\mathbf{0}, \Delta\mathbf{x}) \mathbf{u}^0 = \mathbf{f}$
 Assemble $\mathbf{f}^0 := \mathbf{f} - \mathbf{A}(\mathbf{u}^0, \Delta\mathbf{x}) \mathbf{u}^0$
while $\|\mathbf{f}^i\|/\|\mathbf{f}\| > \text{precision}$ **do**
 $i := i + 1$
 Solve $\mathbf{A}'_{\mathbf{u}}(\mathbf{u}^{i-1}, \Delta\mathbf{x}) \mathbf{w}^i = \mathbf{f}^{i-1}$
 Find τ^i : $\|\mathbf{f} - \mathbf{A}(\mathbf{u}^{i-1} + \tau^i \mathbf{w}^i, \Delta\mathbf{x}) (\mathbf{u}^{i-1} + \tau^i \mathbf{w}^i)\| < \mathbf{f}^{i-1}$
 $\mathbf{u}^i := \mathbf{u}^{i-1} + \tau^i \mathbf{w}^i$
 $\mathbf{f}^i := \mathbf{f} - \mathbf{A}(\mathbf{u}^i, \Delta\mathbf{x}) \mathbf{u}^i$
 Store \mathbf{w}^i and τ^i
end while
 Store \mathbf{u}^i
 Store $k := i$
 Calculate objective $I(\mathbf{u}^k)$

where ν is defined by (2) and where

$$\mathbf{B}^e(\Delta\mathbf{x}^e) := (\mathbf{R}^e(\Delta\mathbf{x}^e))^{-T} \mathbf{B}^r, \quad \mathbf{R}^e(\Delta\mathbf{x}^e) := (\mathbf{x}_3^e - \mathbf{x}_1^e, \mathbf{x}_2^e - \mathbf{x}_1^e),$$

$$\mathbf{x}_i^e := \mathbf{x}^{\text{init}_i^e} + \Delta\mathbf{x}_i^e.$$

Then, the linearization is assembled out of

$$\begin{aligned} \mathbf{A}'_{\mathbf{u}^e}(\mathbf{u}^e, \Delta\mathbf{x}^e) &= (\mathbf{B}^e(\Delta\mathbf{x}^e))^T \left\{ \left[\nu(\|\mathbf{B}^e(\Delta\mathbf{x}^e)\mathbf{u}^e\|^2, 1) \mathbf{I} \right. \right. \\ &\quad \left. \left. + 2\nu'_{\eta^e}(\|\mathbf{B}^e(\Delta\mathbf{x}^e)\mathbf{u}^e\|^2, 1) (\mathbf{B}^e(\Delta\mathbf{x}^e)\mathbf{u}^e) (\mathbf{B}^e(\Delta\mathbf{x}^e)\mathbf{u}^e)^T \right] \mathbf{B}^e(\Delta\mathbf{x}^e) \right\} \\ &\quad \times \frac{|\det(\mathbf{R}^e(\Delta\mathbf{x}^e))|}{2}. \end{aligned} \tag{13}$$

4.2 Shape sensitivity analysis

For the very outer optimization iterations, we use a quasi-Newton method, for which we need to evaluate the derivative of the cost functional I subject to the design \mathbf{p} . Similarly to Section 2.2, we analytically differentiate Algorithm 3 in the backward way, which arises in Algorithm 4. The new matrices are as follows:

$$\begin{aligned} \mathbf{G}_{\Delta\mathbf{x}}(\mathbf{u}, \mathbf{w}, \Delta\mathbf{x}) &:= \\ &- \left(\frac{\partial \mathbf{A}'_{\mathbf{u}}(\mathbf{u}, \Delta\mathbf{x})}{\partial \Delta x_{1,1}} \mathbf{w}, \frac{\partial \mathbf{A}'_{\mathbf{u}}(\mathbf{u}, \Delta\mathbf{x})}{\partial \Delta x_{1,2}} \mathbf{w}, \dots, \frac{\partial \mathbf{A}'_{\mathbf{u}}(\mathbf{u}, \Delta\mathbf{x})}{\partial \Delta x_{n,1}} \mathbf{w}, \frac{\partial \mathbf{A}'_{\mathbf{u}}(\mathbf{u}, \Delta\mathbf{x})}{\partial \Delta x_{n,2}} \mathbf{w} \right) \\ &- \left(\frac{\partial \mathbf{A}(\mathbf{u}, \Delta\mathbf{x})}{\partial \Delta x_{1,1}} \mathbf{u}, \frac{\partial \mathbf{A}(\mathbf{u}, \Delta\mathbf{x})}{\partial \Delta x_{1,2}} \mathbf{u}, \dots, \frac{\partial \mathbf{A}(\mathbf{u}, \Delta\mathbf{x})}{\partial \Delta x_{n,1}} \mathbf{u}, \frac{\partial \mathbf{A}(\mathbf{u}, \Delta\mathbf{x})}{\partial \Delta x_{n,2}} \mathbf{u} \right), \end{aligned}$$

Algorithm 4 Adjoint Newton method for shape optimization

Given \mathbf{p} , $\Delta\boldsymbol{\alpha}$, $\Delta\mathbf{x}$, k , \mathbf{u}^k , $\{\mathbf{w}^i\}_{i=1}^k$ and $\{\tau^i\}_{i=1}^k$ stored by Algorithm 3

$\boldsymbol{\lambda} := I'_{\mathbf{u}}(\mathbf{u}^k)$

$\boldsymbol{\omega} := \mathbf{0}$

for $i = k, \dots, 1$ **do**

$\mathbf{u}^{i-1} := \mathbf{u}^i - \tau^i \mathbf{w}^i$

Solve $\mathbf{A}'_{\mathbf{u}}(\mathbf{u}^{i-1}, \Delta\mathbf{x})^T \boldsymbol{\eta} = \boldsymbol{\lambda}$

Assemble $\boldsymbol{\omega} := \boldsymbol{\omega} + \tau^i \mathbf{G}_{\Delta\mathbf{x}}(\mathbf{u}^{i-1}, \mathbf{w}^i, \Delta\mathbf{x})^T \boldsymbol{\eta}$

Assemble $\boldsymbol{\lambda} := \boldsymbol{\lambda} + \tau^i \mathbf{G}_{\mathbf{u}}(\mathbf{u}^{i-1}, \mathbf{w}^i, \Delta\mathbf{x})^T \boldsymbol{\eta}$

end for

Solve $\mathbf{A}(\mathbf{0}, \Delta\mathbf{x})^T \boldsymbol{\eta} = \boldsymbol{\lambda}$

Assemble $\boldsymbol{\omega} := \boldsymbol{\omega} + \mathbf{H}_{\Delta\mathbf{x}}(\mathbf{u}^0, \Delta\mathbf{x})^T \boldsymbol{\eta}$

Solve $(\mathbf{K}^{\text{stiff}} + p_{\alpha} \mathbf{K}^{\text{robin}})^T \boldsymbol{\eta} = \boldsymbol{\omega}$

$\boldsymbol{\theta} := (p_{\alpha} \mathbf{K}^{\text{robin}} \mathbf{M})^T \boldsymbol{\eta}$

Calculate the gradient of the objective $I'_{\mathbf{p}}(\mathbf{u}^k(\Delta\mathbf{x}(\boldsymbol{\alpha}(\mathbf{p})))) := \boldsymbol{\alpha}'_{\mathbf{p}}(\mathbf{p}) \boldsymbol{\theta}$

$$\begin{aligned} \mathbf{G}_{\mathbf{u}}(\mathbf{u}, \mathbf{w}, \Delta\mathbf{x}) := & - \left(\frac{\partial \mathbf{A}'_{\mathbf{u}}(\mathbf{u}, \Delta\mathbf{x})}{\partial u_1} \mathbf{w}, \dots, \frac{\partial \mathbf{A}'_{\mathbf{u}}(\mathbf{u}, \Delta\mathbf{x})}{\partial u_n} \mathbf{w} \right) \\ & - \left(\frac{\partial \mathbf{A}(\mathbf{u}, \Delta\mathbf{x})}{\partial u_1} \mathbf{u}, \dots, \frac{\partial \mathbf{A}(\mathbf{u}, \Delta\mathbf{x})}{\partial u_n} \mathbf{u} \right) - \mathbf{A}(\mathbf{u}, \Delta\mathbf{x}), \end{aligned}$$

$$\begin{aligned} \mathbf{H}_{\Delta\mathbf{x}}(\mathbf{u}, \Delta\mathbf{x}) := & - \left(\frac{\partial \mathbf{A}(\mathbf{0}, \Delta\mathbf{x})}{\partial \Delta x_{1,1}} \mathbf{u}, \frac{\partial \mathbf{A}(\mathbf{0}, \Delta\mathbf{x})}{\partial \Delta x_{1,2}} \mathbf{u}, \dots, \frac{\partial \mathbf{A}(\mathbf{0}, \Delta\mathbf{x})}{\partial \Delta x_{n,1}} \mathbf{u}, \frac{\partial \mathbf{A}(\mathbf{0}, \Delta\mathbf{x})}{\partial \Delta x_{n,2}} \mathbf{u} \right) \end{aligned}$$

so that they are assembled elementwise out of

$$\begin{aligned} \frac{\partial \mathbf{A}^e(\mathbf{u}^e, \Delta x_{i,j}^e)}{\partial \Delta x_{i,j}^e} = & \left(\frac{\partial \mathbf{B}^e}{\partial \Delta x_{i,j}^e} \right)^T [\nu^e \mathbf{I}] \mathbf{B}^e \frac{|\det(\mathbf{R}^e)|}{2} \\ & + (\mathbf{B}^e)^T [\nu^e \mathbf{I}] \frac{\partial \mathbf{B}^e}{\partial \Delta x_{i,j}^e} \frac{|\det(\mathbf{R}^e)|}{2} \\ & + (\mathbf{B}^e)^T \left[\frac{\nu^{e'}}{\|\mathbf{B}^e \mathbf{u}^e\|} \left(\frac{\partial \mathbf{B}^e}{\partial \Delta x_{i,j}^e} \mathbf{u}^e \right)^T (\mathbf{B}^e \mathbf{u}^e) \mathbf{I} \right] \mathbf{B}^e \frac{|\det(\mathbf{R}^e)|}{2} \\ & + (\mathbf{B}^e)^T \left[\frac{\nu^{e'}}{\|\mathbf{B}^e \mathbf{u}^e\|} \mathbf{I} \right] \mathbf{B}^e \frac{\text{sign}(\det(\mathbf{R}^e))}{2} \frac{\partial \det(\mathbf{R}^e)}{\partial \Delta x_{i,j}^e}, \end{aligned}$$

$$\begin{aligned}
\frac{\partial \mathbf{A}_{\mathbf{u}^e}^{e'}(\mathbf{u}^e, \Delta x_{i,j}^e)}{\partial \Delta x_{i,j}^e} = & \left(\frac{\partial \mathbf{B}^e}{\partial \Delta x_{i,j}^e} \right)^T \left[\nu^{e'} \mathbf{I} + \frac{\nu^{e'}}{\|\mathbf{B}^e \mathbf{u}^e\|} (\mathbf{B}^e \mathbf{u}^e) (\mathbf{B}^e \mathbf{u}^e)^T \right] \mathbf{B}^e \frac{|\det(\mathbf{R}^e)|}{2} \\
& + (\mathbf{B}^e)^T \left[\nu^{e'} \mathbf{I} + \frac{\nu^{e'}}{\|\mathbf{B}^e \mathbf{u}^e\|} (\mathbf{B}^e \mathbf{u}^e) (\mathbf{B}^e \mathbf{u}^e)^T \right] \frac{\partial \mathbf{B}^e}{\partial \Delta x_{i,j}^e} \frac{|\det(\mathbf{R}^e)|}{2} \\
& + (\mathbf{B}^e)^T \left[\nu^{e'} \mathbf{I} + \frac{\nu^{e'}}{\|\mathbf{B}^e \mathbf{u}^e\|} (\mathbf{B}^e \mathbf{u}^e) (\mathbf{B}^e \mathbf{u}^e)^T \right] \mathbf{B}^e \frac{\text{sign}(\det(\mathbf{R}^e))}{2} \frac{\partial \det(\mathbf{R}^e)}{\partial \Delta x_{i,j}^e} \\
& + (\mathbf{B}^e)^T \left[\frac{\nu^{e'}}{\|\mathbf{B}^e \mathbf{u}^e\|} (\mathbf{B}^e \mathbf{u}^e)^T (\mathbf{B}^e \mathbf{u}^e) \mathbf{I} \right. \\
& \quad \left. + \left(\frac{\nu^{e''}}{\|\mathbf{B}^e \mathbf{u}^e\|^2} - \frac{\nu^{e'}}{\|\mathbf{B}^e \mathbf{u}^e\|^3} \right) \left\{ \left(\frac{\partial \mathbf{B}^e}{\partial \Delta x_{i,j}^e} \mathbf{u}^e \right)^T (\mathbf{B}^e \mathbf{u}^e) \right\} (\mathbf{B}^e \mathbf{u}^e) (\mathbf{B}^e \mathbf{u}^e)^T \right. \\
& \quad \left. + \frac{\nu^{e'}}{\|\mathbf{B}^e \mathbf{u}^e\|} \left\{ \left(\frac{\partial \mathbf{B}^e}{\partial \Delta x_{i,j}^e} \mathbf{u}^e \right) (\mathbf{B}^e \mathbf{u}^e)^T \right. \right. \\
& \quad \quad \left. \left. + (\mathbf{B}^e \mathbf{u}^e) \left(\frac{\partial \mathbf{B}^e}{\partial \Delta x_{i,j}^e} \mathbf{u}^e \right)^T \right\} \right] \mathbf{B}^e \frac{|\det(\mathbf{R}^e)|}{2},
\end{aligned}$$

where $i = 1, 2, \dots, n$ are nodal indices, $j = 1, 2$ are coordinates indices and where we simplified the notation by $\mathbf{B}^e := \mathbf{B}^e(\Delta \mathbf{x}^e)$, $\mathbf{R}^e := \mathbf{R}^e(\Delta \mathbf{x}^e)$, $\nu^e := \nu^e(\|\mathbf{B}^e \mathbf{u}^e\|^2, 1)$, $\nu^{e'} := \nu_{\eta^e}^{e'}(\|\mathbf{B}^e \mathbf{u}^e\|^2, 1)$ and $\nu^{e''} := \nu_{\eta^e \eta^e}^{e''}(\|\mathbf{B}^e \mathbf{u}^e\|^2, 1)$. Finally, the expression for $\mathbf{G}_{\mathbf{u}^e}^e(\mathbf{u}^e, \mathbf{w}^e, \Delta \mathbf{x}^e)$ is given by (6), where now $\tilde{\rho}^e := 1$.

4.3 Multilevel shape optimization

Besides the sensitivity analysis presented above, the most speed-up of the algorithm is performed by using a multilevel approach, which we present in Algorithm 5. There, we propose to couple the very outer quasi-Newton optimization method with the nested Newton method for elimination the nonlinear state problem. At each iteration of Algorithm 3, the conjugate gradients method is employed so that only one preconditioner per level is used; for the system matrix \mathbf{A} as well as for its linearization $\mathbf{A}'_{\mathbf{u}^e}$. The preconditioner is successively built in the geometric-multigrid way. At the first level, we use a direct solver and, at the end, for the first-level optimized design we store the inverse of the system matrix \mathbf{A} to be the coarsest grid preconditioner. After optimization at the second level we store the second grid corrections of the preconditioner so that we consider the second-level optimized design, etc. In Algorithm 3, we denote by $\mathcal{A}^{(l)}(\mathbf{p}_1^{(l)}, \dots, \mathbf{p}_s^{(l)})$ the matrix $\mathbf{A}(\mathbf{u}(\Delta \mathbf{x}(\boldsymbol{\alpha}(\mathbf{p}^{(l)}))), \Delta \mathbf{x}(\boldsymbol{\alpha}(\mathbf{p}^{(l)})))$, which is discretized and assembled at the level l for the design $\mathbf{p}^{(l)} := [\mathbf{p}_1^{(l)}, \dots, \mathbf{p}_s^{(l)}]$.

The third important issue improving the speed-up is that we use the optimized design as the initial one at the next optimization level. Note that in each run of both the state elimination and the adjoint method one solution to the system (11) is involved. Here, we again use the conjugate gradients method preconditioned by a geometric multigrid. However, the operator $\mathbf{K}^{\text{stiff}} + p_\alpha \mathbf{K}^{\text{robin}}$ is not perturbed by design changes, unlike the operator \mathbf{A} , and the solution is indeed optimal.

Algorithm 5 Multilevel shape optimization

Given $\mathbf{p}_1^{(1),\text{init}}, \dots, \mathbf{p}_s^{(1),\text{init}}$

Discretize at the first level $\rightarrow h^{(1)}, \mathcal{A}^{(1)}(\mathbf{p}_1^{(1),\text{init}}, \dots, \mathbf{p}_s^{(1),\text{init}})$

Solve by a quasi-Newton method coupled with Algorithm 3, while using a nested direct solver: $\mathbf{p}_1^{(1),\text{init}}, \dots, \mathbf{p}_s^{(1),\text{init}} \rightarrow \mathbf{p}_1^{(1),\text{opt}}, \dots, \mathbf{p}_s^{(1),\text{opt}}$

Store the first level preconditioner $\mathcal{C}^{(1)} := [\mathcal{A}^{(1)}(\mathbf{p}_1^{(1),\text{opt}}, \dots, \mathbf{p}_s^{(1),\text{opt}})]^{-1}$

for $l = 2, \dots$ **do**

Refine: $h^{(l-1)} \rightarrow h^{(l)}$

Prolong: $\mathbf{p}_1^{(l-1),\text{opt}}, \dots, \mathbf{p}_s^{(l-1),\text{opt}} \rightarrow \mathbf{p}_1^{(l),\text{init}}, \dots, \mathbf{p}_s^{(l),\text{init}}$

Solve by a quasi-Newton method coupled with Algorithm 3, while using the nested conjugate gradients method preconditioned with $\mathcal{C}^{(l-1)}$:

$\mathbf{p}_1^{(l),\text{init}}, \dots, \mathbf{p}_s^{(l),\text{init}} \rightarrow \mathbf{p}_1^{(l),\text{opt}}, \dots, \mathbf{p}_s^{(l),\text{opt}}$

Store the l -th level multigrid preconditioner $\mathcal{C}^{(l)} \approx [\mathcal{A}^{(l)}(\mathbf{p}_1^{(l)}, \dots, \mathbf{p}_s^{(l)})]^{-1}$

end for

5 Optimal design of an electromagnet

We consider a direct electric current (DC) electromagnet, see Fig. 2. Such electromagnets are used for measurements of Kerr magneto-optic effects, cf. [ZK97]. They require the magnetic field among the pole heads as homogeneous as possible. Let us note that the magneto-optic effects are investigated for applications in high capacity data storage media, like development of new media materials for magnetic or compact discs recording. Let us also note that the electromagnets have been developed at the Institute of Physics, Technical University of Ostrava, Czech Republic, see [Pos02]. A number of instances have been delivered to laboratories in France, Canada or Japan.

Our aim is to improve the current geometries of the electromagnets in order to be better suited for measurements of the Kerr effect. The generated magnetic field should be strong and homogeneous enough. Unfortunately, these assumptions are contradictory and we have to balance them. The cost functional reads as follows:

$$\mathcal{I}(u) := \int_{\Omega_m} \|\mathbf{curl}(u) - B_m^{\text{avg}}(u)\mathbf{n}_m\|^2 dx + p_B (\min\{0, B_m^{\text{avg}}(u) - B^{\text{min}}\})^2,$$

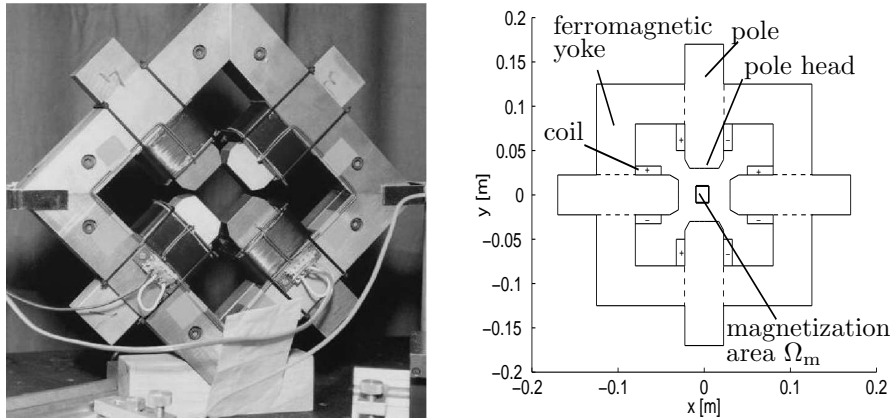


Figure 2: An electromagnet of the Maltese Cross geometry

where $\Omega_m \subset \Omega$ is the subdomain where the magnetic field should be homogeneous, $\mathbf{curl}(u) := (\partial u / \partial x_2, -\partial u / \partial x_1)$, $B_m^{\text{avg}}(u)$ is the mean value of the magnetic field component $\mathbf{curl}(u)\mathbf{n}_m$ over Ω_m , $\mathbf{n}_m := (0, 1)$, $B^{\text{min}} := 0.12$ [T] is the required minimal field and $p_B := 10^6$ is the penalty of the minimal field constraint. There are 600 turns pumped by the current of 5 [A], which is averaged into a current density J being constant in the coil subdomain and vanishing elsewhere. The relative permeability of the used ferromagnetics is 5100, the linearized relative reluctivity in (2) is then $\nu_1 := \nu_0/5100$. This application was already closely discussed in [Luk01, Luk04], where we considered shape optimization governed with the linear state problem only.

6 Numerical results

The presented results were achieved using the software Netgen/NgSolve developed at the University Linz, Austria, in the group of Joachim Schöberl, cf. [KLS00, Sch97]. We consider our 2D application, where, for simplicity, only two coils are active so that we can take, due to the symmetry, a quarter of the domain, see Fig. 3. Given the initial design $\rho^{\text{init}} := 0.5$ in Ω_d , we start with the topology optimization. Concerning (3), we choose $V_{\text{max}} := 0.0155$ [m²] and $p_V := 100$. A coarse optimized topology design is depicted in Fig. 4. There are 861 design, 1105 state variables and the optimization was done in 7 steepest descent iterations which took 2.5 seconds, when using the adjoint method for the sensitivity analysis.

The second part of the computation is the shape approximation. Here, we refer to Fig. 5. We are looking for three Bézier curves that fit the optimized topology. There are 19 design parameters in total and solving the least square problem (8) was finished in 8 quasi-Newton iterations, which took 26 seconds when using numerical differentiation.

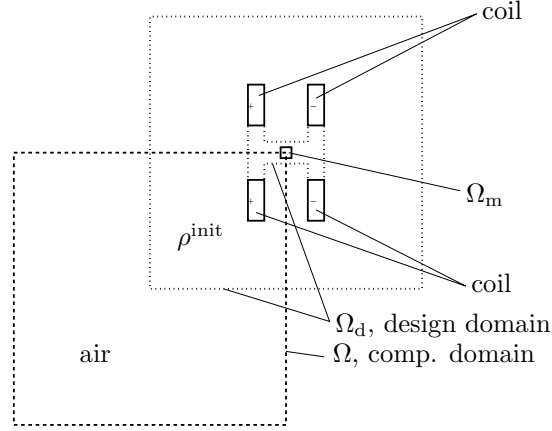


Figure 3: Initial design for the topology optimization

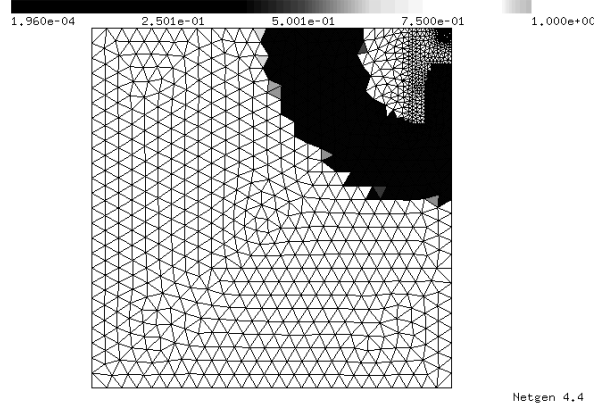


Figure 4: Coarsely optimized topology design ρ^{opt}

Finally, we used the smooth shape design as the initial guess for the shape optimization (10). Table 1 depicts parameters of the computation. At each level, we refined uniformly the state as well as the design space. The number of the outer optimization iterations seems to be independent of the level, which is caused by using the coarsely optimized design as the initial starting point at the next level. The fifth column shows the numbers of the inner Newton iterations necessary for elimination of the nonlinear state problem. The stability of these numbers is given by the kind of nonlinearity we have, see also (2). The sixth column is perhaps the most interesting one, since it shows the performance of the multigrid. We can see that the linear system with the operator $\mathbf{A}(\mathbf{0}, \Delta \mathbf{x})$ was solved almost in the optimal way (6 iterations at worst), however, solution to the linearized system $\mathbf{A}'_{\mathbf{u}}(\mathbf{u}^{i-1}, \Delta \mathbf{x})$ is by far less efficient. This is due to the fact that we only used the preconditioner for the linear part, which did

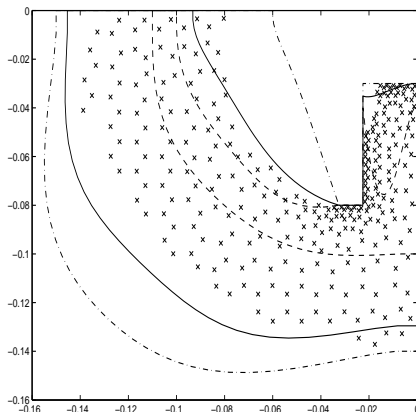


Figure 5: Shape approximation: dashed line – lower bound; dash-and-dot line – upper bound; solid line – optimal shape approximation; crosses – mid-points of the elements with $\rho^{\text{opt}} \geq 0.5$

Table 1: Multilevel shape optimization

level	design variables	outer iters.	state variables	max. inner iters.	CG steps lin./nonlin.	time
1	19	10	1098	3	direct	32s
2	40	15	4240	3	3/14–25	2min 52s
3	82	9	16659	4	4–5/9–48	9min 3s
4	166	10	66037	4	4–6/13–88	49min 29s
5	334	13	262953	5	3–6/20–80	6h 36min

not bring any extra cost. From the last column, we can see that a large-scale shape optimization can be solved in terms of minutes. The final optimized geometry is depicted in Fig. 6 (a). We can see that the result is in a good correspondance with the so-called O-Ring electromagnet, which was already designed and manufactured by physicists.

7 Conclusion

This paper presented a method which sequentially combines topology and shape optimization. First, we solved a coarsely discretized topology optimization problem. Then, we approximated some chosen interfaces by Bézier shapes. Finally, we proceeded with shape optimization in a multilevel way. We applied the method to a 2D optimal shape design of a DC electromagnet. We get fine optimized geometries in minutes. It remains to analyze and improve the multigrid convergence, particularly, in case of the nonlinear state operator.

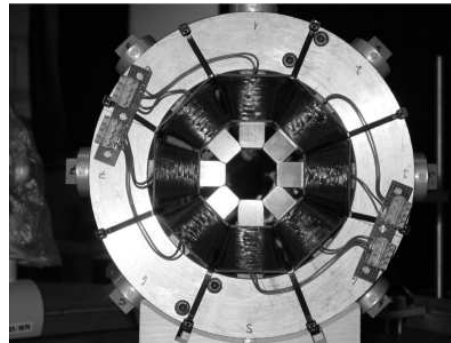
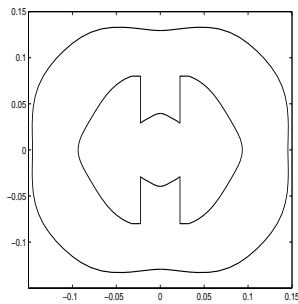


Figure 6: Multilevel shape optimization: (a) optimized geometry; (b) the O-Ring electromagnet

Acknowledgement

The authors would like to thank to Prof. Ulrich Langer and Dr. Martin Burger from University Linz, Austria, for their valuable suggestions.

References

- [Ben95] Bendsøe, M.P.: Optimization of Structural Topology, Shape and Material. Springer, Berlin, Heidelberg (1995)
- [Bra93] Bramble, J.H.: Multigrid Methods. Wiley (1993)
- [Cea00] C ea, J., Garreau, S., Guillaume, P., Masmoudi, M.: The shape and topological optimizations connection. *Comput. Methods Appl. Mech. Eng.* **188**, 713–726 (2000)
- [SMS00] Dreyer, T., Maar, B., Schulz, V.: Multigrid optimization in applications. *J. Comp. Appl. Math.* **120**, 67–84 (2000)
- [Far96] Farin, G.E.: Curves and Surfaces for Computer–Aided Geometric Design: A Practical Guide. Academic Press (1996)
- [Gri00] Griewank, A.: Evaluating Derivatives, Principles and Techniques of Algorithmic Differentiation. SIAM (2000)
- [Hac85] Hackbusch, W.: Multi–grid Methods and Applications. Springer (1985)
- [HN97] Haslinger J., Neittaanm aki P.: Finite Element Approximation for Optimal Shape, Material and Topology Design. Wiley, Chichester (1997)
- [HCK86] Haug, E.J., Choi, K.K., Komkov, V.: Sensitivity Analysis in Structural Design. Academic Press (1986)

- [JL85] Jung, M., Langer, U.: Methode der finiten Elemente für Ingenieure: Eine Einführung in die numerischen Grundlagen und Computersimulation. Teubner (2001)
- [Luk01] Lukáš, D.: Shape optimization of homogeneous electromagnets. In: van Rienen, U., Günther, M., Hecht, D. (eds.) Scientific Computing in Electrical Engineering 2000, Lect. Notes Comp. Sci. Engrg. **18**, 145–152 (2001)
- [Luk04] Lukáš, D.: On solution to an optimal shape design problem in 3-dimensional linear magnetostatics. Appl. Math. **49**:5, 441–464 (2004)
- [KLS00] Kuhn, M., Langer, U., Schöberl, J.: Scientific computing tools for 3d magnetic field problems, MAFELAP **10**, 239–259 (2000)
- [OBR91] Olhoff, N., Bendsøe, M.P., Rasmussen, J.: On CAD-integrated structural topology and design optimization. Comp. Meth. Appl. Mech. Eng. **89**, 259–279 (1991)
- [Pos02] Postava, K., Hrabovský, D., Pištora, J., Fert, A.R., Višňovský, Š., Yamaguchi, T.: Anisotropy of quadratic magneto-optic effects in reflection. J. Appl. Phys. **91**, 7293–7295 (2002)
- [Sch97] Schöberl, J.: NETGEN – an advancing front 2d/3d-mesh generator based on abstract rules. Comp. Vis. Sci. **1**, 41–52 (1997)
- [SZ92] Sokolowski, J., Zolesio, J.-P.: Introduction to Shape Optimization. Springer (1992)
- [TCh01] Tang, P.-S., Chang, K.-H.: Integration of topology and shape optimization for design of structural components. Struct. Multidisc. Optim. **22**, 65–82 (2001)
- [ZK97] Zvedin, A.K., Kotov, V.A.: Modern Magneto-optics and Magneto-optical Materials. Institute of Physics Publishing Bristol and Philadelphia (1997)